This article was downloaded by: *[EPFL Lausanne]*
On: *25 March 2011*
Access details: *Access Details: [subscription number 919488055]*
Publisher *Taylor & Francis*
Informa Ltd Registered in England and Wales Registered Number: 1072954 Registered office: Mortimer House, 37-41 Mortimer Street, London W1T 3JH, UK

Journal of Dispersion Science and Technology
Publication details, including instructions for authors and subscription information:
http://www.informaworld.com/smpp/title~content=t713597266

Hamaker 2: A Toolkit for the Calculation of Particle Interactions and Suspension Stability and its Application to Mullite Synthesis by Colloidal Methods

Ulrich Aschauer[a]; Olga Burgos-Montes[b]; Rodrigo Moreno[b]; Paul Bowen[a]
[a] Laboratoire de Technologie des Poudres, Ecole Polytechnique Fédérale de Lausanne (EPFL), Lausanne, Switzerland [b] Instituto de cerámica y Vidro, Consejo Superior de Investigaciones Científicas (CSIC), Madrid, Spain

Online publication date: 24 March 2011

To cite this Article Aschauer, Ulrich , Burgos-Montes, Olga , Moreno, Rodrigo and Bowen, Paul(2011) 'Hamaker 2: A Toolkit for the Calculation of Particle Interactions and Suspension Stability and its Application to Mullite Synthesis by Colloidal Methods', Journal of Dispersion Science and Technology, 32: 4, 470 — 479
To link to this Article: DOI: 10.1080/01932691003756738
URL: http://dx.doi.org/10.1080/01932691003756738

PLEASE SCROLL DOWN FOR ARTICLE

Full terms and conditions of use: http://www.informaworld.com/terms-and-conditions-of-access.pdf

This article may be used for research, teaching and private study purposes. Any substantial or systematic reproduction, re-distribution, re-selling, loan or sub-licensing, systematic supply or distribution in any form to anyone is expressly forbidden.

The publisher does not give any warranty express or implied or make any representation that the contents will be complete or accurate or up to date. The accuracy of any instructions, formulae and drug doses should be independently verified with primary sources. The publisher shall not be liable for any loss, actions, claims, proceedings, demand or costs or damages whatsoever or howsoever caused arising directly or indirectly in connection with or arising out of the use of this material.

Journal of Dispersion Science and Technology, 32:470–479, 2011
Copyright © Taylor & Francis Group, LLC
ISSN: 0193-2691 print/1532-2351 online
DOI: 10.1080/01932691003756738

Taylor & Francis
Taylor & Francis Group

Hamaker 2: A Toolkit for the Calculation of Particle Interactions and Suspension Stability and its Application to Mullite Synthesis by Colloidal Methods

Ulrich Aschauer,[1] Olga Burgos-Montes,[2] Rodrigo Moreno,[2] and Paul Bowen[1]

[1]*Laboratoire de Technologie des Poudres, Ecole Polytechnique Fédérale de Lausanne (EPFL), Lausanne, Switzerland*
[2]*Instituto de cerámica y Vidro, Consejo Superior de Investigaciones Científicas (CSIC), Madrid, Spain*

For modern processing of ceramics at the nanoscale, the influence of interparticle interactions in the suspended state becomes increasingly important. The Hamaker 2 program has been developed for the rapid prediction of these interactions, allowing us to gain important understanding of the often delicate balance of forces in ceramic powder suspensions. This article discusses the theoretical foundation of the implemented models and shows the benefit of this predictive approach applied to mullite production by colloidal methods.

Keywords DLVO theory, mullite, software, suspension stability

Downloaded By: [EPFL Lausanne] At: 10:13 25 March 2011

1. INTRODUCTION

In modern ceramic technology, interparticle interactions in the suspended state are of increasing importance for optimum quality in experimental and industrial applications.[1] Cases where these interactions are of importance are, among others, the fabrication of high quality green bodies, for highly transparent ceramics,[2,3] or colloidal preparation routes for advanced powders, for example, by hetero coagulation.[4] Ceramic thin or thick films for porous films for ink-jet paper coatings[5] and piezoelectric screen printing applications[6] also depend greatly on the rheological properties and quality of dispersion. Interparticle forces also play a major role in the workability of cement and concrete pastes.[7] The modern use of sophisticated polymers to enhance dispersion and workability of cementitious materials is a key factor in the improved mechanical behavior and in the use of alternative more environmentally friendly cement substitutes.[8]

In all of these cases, one would like to tune experimentally accessible parameters of both the powder and suspension medium in order to obtain either good dispersion or coagulation for the entire system or parts of it. The interplay of the different parameters is, however, often difficult to understand without resorting to theoretical approaches, which has led to many publications,[7,9–14] where interparticle interaction calculations were used to predict or explain experiment.

Although these approaches have been used for many years and applied with success,[15] it would often be helpful to have a tool to rapidly carry out these calculations without having to implement the models from scratch. It is in this perspective that the freely available Hamaker code was developed (download at http://hamaker.epfl.ch). The goal was a program with a graphical user interface to allow rapid evaluation of interparticle interactions, however, without limiting more complex aspects required by advanced users. The software should also be extensible at the user level by means of plug-in modules to allow the easy inclusion of new interactions as the need arises. In this article, we outline the theoretical foundations on which the code relies as well as implementation highlights. We then demonstrate the usefulness of the code by a detailed case study for the production of mullite via a heterocoagulation route and compare with experimental results.

Received 9 December 2009; accepted 10 January 2010.

Present affiliation for U. A.: Department of Chemistry, Princeton University, Princeton, USA.

Present affiliation for O. B.-M.: Instituto Eduardo Torroja, CSIC, Madrid, Spain.

Address correspondence to Ulrich Aschauer, Department of Chemistry, Princeton University, Frick Laboratory, Princeton, NJ 08544, USA. E-mail: aschauer@princeton.edu

2. THEORY

The interaction models built into the code predict interparticle interactions within the DLVO[16,17] theory with an extension to treat steric repulsion forces. The code calculates the total interaction potential V as a sum

Downloaded By: [EPFL Lausanne] At: 10:13 25 March 2011

of attractive dispersion interactions V_{disp}, repulsive electrostatic interactions V_{elec} and steric interactions V_{steric} as given by Equation (1).

$$V = V_{disp} + V_{elec} + V_{steric} + \sum V_{user}. \quad [1]$$

Arbitrary interaction potentials V_{user} can be added to these standard ones by the user. The models built into the code will briefly be outlined in the following.

2.1. Dispersion Interactions

London dispersion interactions originate from the interaction of temporary dipoles resulting from fluctuations of the charge distribution in a material. In macroscopic bodies every molecule (atom) can be considered as possible dipoles, all of which interact with dipoles in other particles, leading to a rather complicated overall interaction. Hamaker's approach[18] to treat these interactions for macroscopic bodies was to consider a pairwise sum over all molecules (atoms) in the bodies. These sums can be decomposed into the Hamaker constant A_H, which depends on the interacting materials and the medium separating them, as well as a function resulting from the integration over all dipoles, which depends on the geometries of the interacting bodies as well as their separation. For particle-particle interactions are in general approximated with the case of two interacting spheres. For the case of two spherical particles of radii a_1 and a_2 at surface-surface separation h, the interaction potential is given by Equation (2).

$$V_{ham}(h) = -\frac{A_H^{eff}}{6}\left[\frac{2a_1a_2}{h^2+2a_1h+2a_2h} + \frac{2a_1a_2}{(h+2a_1)(h+2a_2)} + \ln\left(\frac{h^2+2a_1h+2a_2h}{(h+2a_1)(h+2a_2)}\right)\right]. \quad [2]$$

Note that, in the equations given in this article, the effective Hamaker constant A_H^{eff} for two different interacting materials in a medium different from vacuum is used. This constant is calculated for a combination of materials as given by Equation (3), where $A_{H,1}^{eff}$ and $A_{H,2}^{eff}$ are the effective Hamaker constants for particle interaction between particles of the same respective material in the medium of interest.

$$A_H^{eff} = \sqrt{A_{H,1}^{eff}A_{H,2}^{eff}}. \quad [3]$$

Effective Hamaker constants for different materials and media can be found in the literature[19] or calculated from spectral data.[20] Hamaker 2 incorporates an online database from which constants for the most common materials can be loaded directly into the program.

The effect the dipoles have on each other travels at the speed of light. Therefore, at large separations a delay in the dipole-dipole interactions is observed and the original model by Hamaker breaks down. Many authors have developed models taking into account this so called retardation effect. In the code the models developed by Vincent[21] and Gregory[22] are implemented.

Vincent's approach applies a correction valid for relatively small separations of small particles to the non retarded Hamaker approach as given by Equation (4).

$$V_{vin}(h) = -\frac{A_{H,eff}}{6}\left\{\begin{array}{l} 1.01\left[\dfrac{2a_1a_2}{h^2+2ha_1+2ha_2} + \dfrac{2a_1a_2}{(h+2a_1)(h+2a_2)} + \ln\left(\dfrac{h^2+2ha_1+2ha_2}{(h+2a_1)(h+2a_2)}\right)\right] \\ + 1.12\dfrac{2\pi}{\lambda}\dfrac{a_1a_2}{a_1+a_2+h}\left[1+\dfrac{h^2+2ha_1+2ha_2+2a_1a_2}{4a_1a_2}\ln\left(\dfrac{h^2+2ha_1+2ha_2}{(h+2a_1)(h+2a_2)}\right)\right] \end{array}\right\}, \quad [4]$$

where λ is the characteristic wave length for the internal molecular motion usually taken as 100 nm.

Gregory applied an empirical method to include the retardation effect, which works well for separations of about one tenth of the particle radius. The formulation is given by Equation (5).

$$V_{gre}(h) = -\frac{A_{H,eff}}{6}\frac{a_1a_2}{h(a_1+a_2)}\left[1-\frac{bh}{\lambda}\ln\left(1+\frac{\lambda}{bh}\right)\right], \quad [5]$$

where $b = 5.32$ is a constant and λ is the characteristic wave length for the internal molecular motion usually taken as 100 nm.

The Hamaker constant can also be calculated based on the dielectric constants and refractive indices and as a function of the separation between the bodies.[15] This model, which includes the retardation effect, is included in the code as of version 2.1. The Hamaker constant is in this case calculated based on the dielectric constant ε and refractive index n of the particles (subscript p) and medium (subscript m) as given by Equation (6) and used in the classical Hamaker equation as given in Equation (2). In Equation (6) ω is the absorption frequency, c the speed of light, k the Boltzmann constant,

and T the temperature.

$$A_H = -\frac{3}{4}kT\left(\frac{\varepsilon_p - \varepsilon_m}{\varepsilon_p + \varepsilon_m}\right)^2 + \frac{3\hbar\omega(n_p^2 - n_m^2)^2}{16\sqrt{2}(n_p^2 + n_m^2)^{3/2}} \times \left\{1 + \left[\frac{\pi n_m}{4\sqrt{2}}\sqrt{n_p^2 + n_m^2}\frac{h\omega}{c}\right]^{3/2}\right\}^{-2/3}. \quad [6]$$

Each of these models has its own range of validity.[23] Whereas the Vincent approach works well for small particles of about 10 nm, the nonretarded approach gives good results between 10 and 100 nm, the Gregory approach being most appropriate at larger separations. The effective Hamaker constant approach finally gives the best results over the whole particle size range.[23]

2.2. Electrostatic Interactions

The code implements two models to take into account the electrostatic interaction of the double layers at the particle surfaces. In the implemented approaches the dispersion medium is characterized by its ionic strength I_c as given by Equation (7).[24]

$$I_c = \frac{1}{2}\sum c_i z_i^2, \quad [7]$$

where c_i is the molar concentration of the ionic species i, having a valence z_i. The double layer formed at the particle surface is characterized by the Debye length κ^{-1} as given by Equation (8).

$$\kappa^{-1} = \sqrt{\frac{\varepsilon\varepsilon_0 kT}{2e^2 I_c 1000 N_A}}. \quad [8]$$

In this equation, ε and ε_0 are the dielectric constant of the medium and the electric constant respectively, k is Boltzmann's constant, T the temperature, e the elementary charge, and N_A Avogadro's constant. The factor 1000 is needed to convert from liters to cubic meters. Based on these basic quantities the following two models are implemented in the code.

The HHF interaction potential by Hogg, Healy, and Fürstenau[25] is based on a linearized Poisson-Boltzmann equation (Debye-Hückel theory), solved using Derjaguin's method and is given by Equation (9). Due to the linearization its validity is limited to small surface potentials (<50–60 mV) and the use of Derjaguin's method imposes the thickness of the double layer and particle-particle separation to be small compared to the particle size.

$$V_{hhf}(h) = \frac{\pi\varepsilon\varepsilon_0 a_1 a_2}{a_1 + a_2}[(\psi_1 + \psi_2)^2 \ln(1 + \exp(-\kappa h)) + (\psi_1 - \psi_2)^2 \ln(1 + \exp(-\kappa h))], \quad [9]$$

where ψ is the surface potential, which can approximately be calculated from the experimentally accessible ζ potential as given by Equation (10), where d_s is the distance from the surface, where the ζ potential is measured. This distance is usually taken as the shear plane, which for an aqueous solution is around 0.5 nm. For solutions containing adsorbing polymers, this value will have to be increased.

$$\psi = \zeta \exp(\kappa d_s). \quad [10]$$

The second model, also based on a linearized Poisson-Boltzmann equation is the linear superposition approximation (LSA)[26] as given by Equation (11). It has the same limitations as the HHF potential except for also being valid at larger separations.

$$V_{lsa}(h) = \frac{4\pi\varepsilon\varepsilon_0 a_1 a_2}{a_1 + a_2 + h}\psi_1\psi_2 \exp(-\kappa h). \quad [11]$$

2.3. Steric Interactions

Hamaker 2 implements at the moment only the close to hard-wall model.[27–29] This model works well for small oligomeres but fails to describe structural effects observed for larger molecules.[30] The interaction potential for this model is divided in three domains, the first being a fully interpenetrated domain at separations closer than the adsorbed layer thickness d_a, where the interaction potential is infinitely repulsive. The code assigns a large value of 10^6 kT rather than infinity in this domain. The interpenetrated domain up to a separation of twice the adsorbed layer thickness is characterized by the molecule-solvent interaction χ, the molecular volume of the solvent V as well as the volume fraction of molecules in the adsorbed layer φ. At larger separations the adsorbed molecules do not interact and the potential is consequently zero.

$$V_{steric}(h) = \begin{cases} h < d_a & : \quad \infty \approx 10^6 \\ d_a \le h \le 2d_a & : \quad \frac{2a_2}{a_1 + a_2}\left[\frac{\pi a_1 kT}{V\varphi^2}(1/2 - \chi)(2d_a - h)^2\right] \\ h > 2d_a & : \quad 0 \end{cases} \quad [12]$$

2.4. Stability Prediction

Hamaker 2 implements the method to estimate the barrier required for suspension stability outlined in Israelachvili.[31] In this method, the mean velocity (v_{mean}) of particles according to a Boltzmann distribution is used together with the average particle-particle spacing (s_{mean}) as obtained via the number of particles per unit volume to estimate the collision frequency (f_{coll}) as given by

Downloaded By: [EPFL Lausanne] At: 10:13 25 March 2011

Equations (13).

$$v_{mean} = \sqrt{\frac{12kT}{\pi d^3 \rho_p}}$$
$$s_{mean} = \left\{ 0.01 c \rho_m \left[4/3\pi \left(\frac{d}{2}\right)^3 \rho_p \right]^{-1} \right\}^{-3}, \qquad [13]$$
$$f_{coll} = \frac{v_{mean}}{s_{mean}}$$

where d is the particle diameter, ρ_p and ρ_m are the densities of particles, and the medium respectively and c is the suspension concentration expressed in wt%. solid/liquid. Within a time t, the number of collisions will be $t \cdot f_{coll}$, and the suspension will be stable if none of these collisions is energetic enough to overcome the primary barrier, thus, avoiding doublet formation. The probability of a single collision to overcome a barrier ΔW is given by $exp(-\Delta W/kT)$. The minimum barrier to avoid doublet formation and consequently agglomeration for a given time t is given by Equation (14).

$$\left(\frac{\Delta W}{kT}\right)_{\min} = -\ln\left(\frac{1}{t \cdot f_{coll}}\right). \qquad [14]$$

It should be noted that this method does not include the effect of any viscous drag the medium exerts on the particles. The present approach is to be considered an upper bound, whereas in reality the required barriers are expected to be slightly lower due to the effect of viscosity.

3. IMPLEMENTATION HIGHLIGHTS

In Hamaker 2 a great deal of attention was put into making plotting as flexible as possible. Plots of the potential and the force between dissimilar particles can be done in two diimensions as a function of a single variable or in three dimensions as a function of two variables. All parameters of the models can be chosen as plotting variables. Moreover, a user-created plug-in model has the possibility to add its variables to the pool of those one can plot against.

These plug-in models make Hamaker 2 very flexible as the user can add virtually any type of interaction potential. Plug-ins implement the mathematical form of interaction potentials and forces as well as any dialog boxes needed to get model parameters from the user. The code comes with a selection of demo plug-in modules, the source code of which can be adapted, allowing even a novice programmer to implement advanced models. These plug-in models are loaded at program start and added to the respective menus to be chosen for interaction calculations.

Hamaker 2 also incorporates a maintained and web-based repository of the often hard to find Hamaker constant. The user can directly load these variables into the code and use them in calculations. Users are encouraged to submit new constants this repository.

4. APPLICATION TO MULLITE PRODUCTION

The mixed oxide ceramic mullite is often produced by starting from the parent oxides Al_2O_3 and SiO_2 followed by a thermal treatment as the process is simple and cost efficient. However for the formation of a homogeneous, high density mullite phase with low defect and secondary phase content during thermal treatment is difficult and a thorough mixing of the two components has to be ensured. Normally mullite is formed only at very high temperatures around 1700–1800°. By using colloidal methods to achieve intimate mixing of nanoparticles of the two oxides, the formation temperature can be lowered, making the process more economical.[32,33]

Here, we report results obtained for suspensions of colloidal silica (specific surface area 200 m^2/g: $d_{v50} = 20$ nm, L200A/40 and L200E/20, Bayer, Germany) stable in basic and acidic environments, respectively, which were mixed with an alumina suspension of mean diameter $d_{v50} =$ 82 nm, resulting from milling a commercial alumina powder (CR125, Baikowski, France). Particle sizes for the suspensions were determined by X-Ray disc centrifuge (XDC, Brookhaven, USA) and specific surface areas S_{BET} by nitrogen adsorption using the BET model (ASAP, Micromiretics, USA). The particle characteristics are given in Table 1, including the average diameter d_{BET} calculated from the S_{BET} and an agglomeration factor, F_{ag} – the ratio between dv_{50} and d_{BET}.[34]

The zeta potentials of the different suspensions were measured using laser Doppler velocimetry (Zetasizer Nano ZS, Malvern, USA) while adjusting the pH with 0.1 M HCl and KOH, respectively. The zeta potential evolution as a

TABLE 1
Characteristics of the silica and alumina particles in suspension

Material	Source	d_{v10} (nm)	d_{v50} (nm)	d_{v90} (nm)	S_{BET} (m^2/g)	d_{BET} (nm)	F_{ag}
SiO_2	L200E/20	3	17	35	200	12	1.4
SiO_2	L200A/40	11	19	31	200	12	1.6
Al_2O_3	CR125	39	82	328	105	15	5.5

Downloaded By: [EPFL Lausanne] At: 10:13 25 March 2011

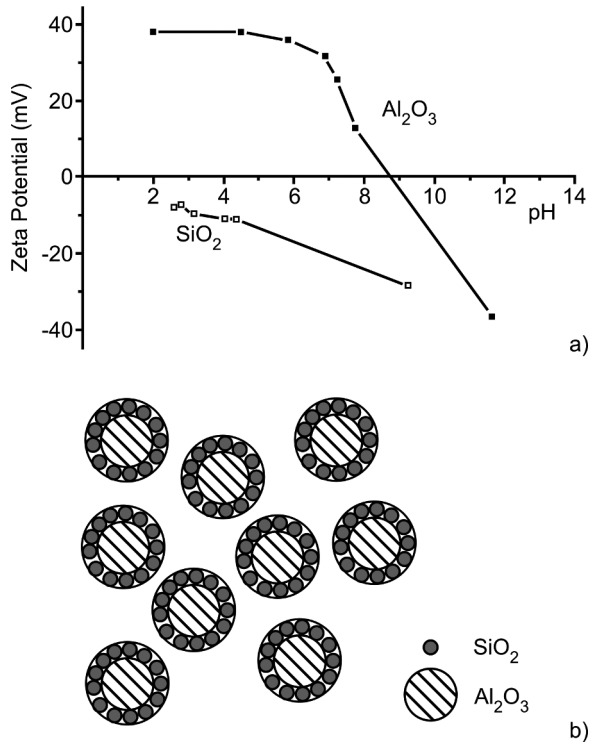

FIG. 1. a) Zeta potential evolution of L200E/20 silica and alumina suspensions. b) Schematic representation of fine silica particles (negative surface charge) coagulated onto alumina core particles (positive surface charge).

function of the pH for the pure silica and alumina suspensions is show in Figure 1a. While alumina shows an isoelectric point (IEP) at around pH 9, silica has a negative zeta potential throughout the whole pH range. This behavior allows the design of two synthesis routes for the production of mullite by mixing of silica and alumina suspensions. At acidic pHs, the surface charges are opposite and heterocoagulation will occur, at basic pHs (>9) the particles will repel each other due to surface charges of the same sign, leading to a well-dispersed suspension. For heterocoagulation to result in a good coverage of the alumina particles by silica ones, by formation of core-shell structure, the relative particle sizes are of great importance. If the silica particles were of similar size, an attractive particle network of high viscosity would result, instead of the intended surface coverage of larger particles (alumina) by the smaller particles (silica) as illustrated schematically in Figure 1b.

The Hamaker 2 software was used to predict the influence of the particle size as well as for the case of the dispersion route the electrosteric effect of an adsorbed polyelectrolyte on the interactions between silica-silica, alumina-alumina, and silica-alumina pairs. The non-retarded dispersion model (Equation (2)) was chosen as most adequate for both particle sizes[23] together with the HHF model (Equation (9)) for the description of electrostatic interactions. All parameters used in the calculations are given in Table 2.

4.1. Heterocoagulation Route

For the heterocoagulation route, one would work in the acidic range to the left of Figure 1a, where the particles carry opposite charges. The pH imposes the use of the L200E/20 silica suspension, which is stable under these conditions. Figure 2 shows the interaction potential between L200E/20 silica-silica and alumina-alumina pairs. Both types of pairs have primary minima at very short separations followed by a positive barrier at separations around 2 nm. The predicted barrier for

TABLE 2
Parameters used in the Hamaker 2 calculations

	Heterocoagulation		Dispersion	
Parameter	Silica L200E/20	Alumina	Silica L200A/40 + PAA	Alumina + PAA*
pH	4	4	8	8
Density (g/cm^3)	2.50	3.997	2.50	3.997
Hamaker constant (10^{-20} J)	0.46	1.60	0.46	1.60
Ionic concentration (M)	0.01	0.01	0.01	0.01
Zeta potential (mV)	−13	+39	−45	−47
d_{v10} (nm)	3	39	11	39
d_{v50} (nm)	17	82	19	82
d_{v90} (nm)	35	328	31	328
Valence (e)	−1	−1	−1	−1
Charge plane (nm)	0	0	0.5	2.5
Dielectric constant	78.54	78.54	78.54	78.54

*Polyacrylic acid needed at basic conditions as discussed in the next section.

Downloaded By: [EPFL Lausanne] At: 10:13 25 March 2011

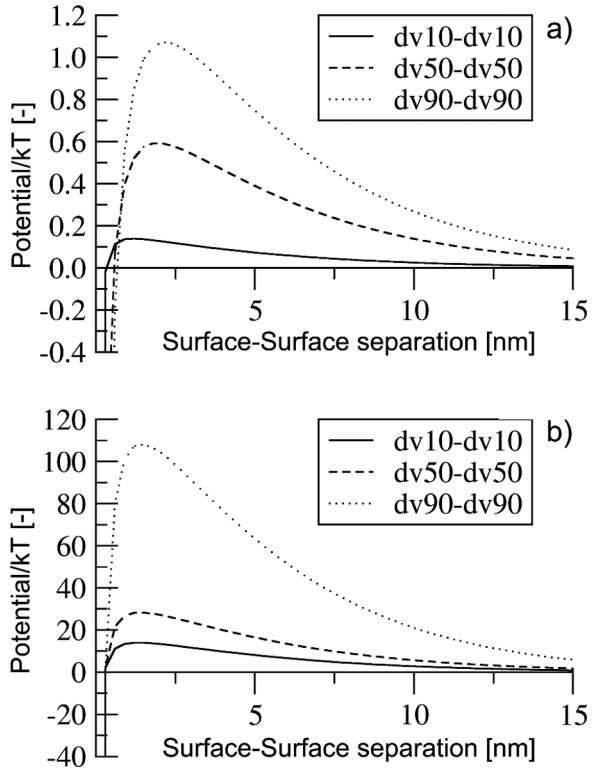

FIG. 2. Interaction potentials for a) silica-silica and b) alumina-alumina pairs.

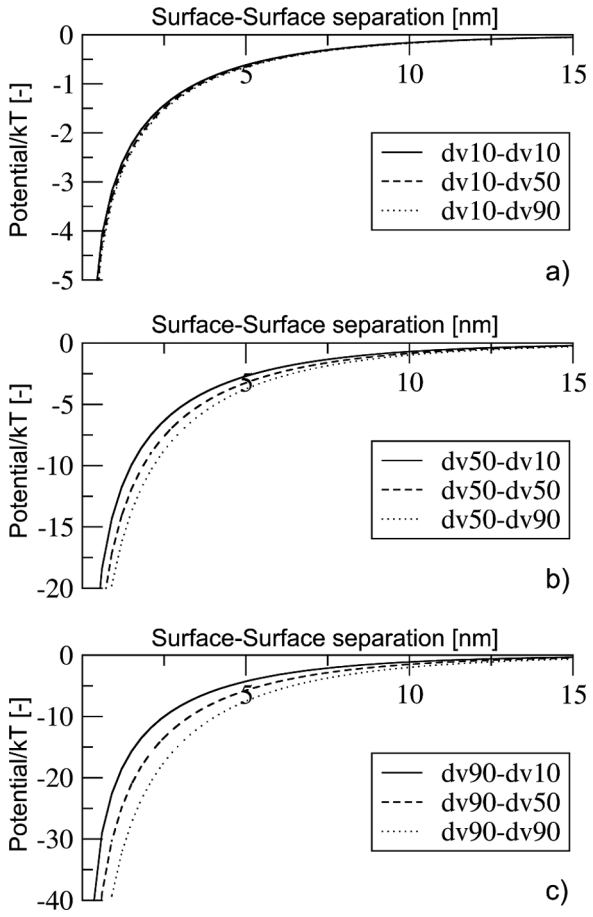

FIG. 3. Interaction potentials for a) silica d_{v10}, b) silica d_{v50}, and c) silica d_{v90} particles with the alumina d_{v10}, d_{v50}, and d_{v90} particles.

alumina pairs is much higher than for the silica pairs due to differences in particle size and zeta potential. The barrier required for stability on the hour timescale is predicted to be around 23 kT showing that there is a slight risk for particles smaller than d_{v50} to agglomerate. For silica-silica pairs the required barrier for stability is about 22 kT and beyond, showing that with the existing barriers smaller than kT severe agglomeration between silica pairs is to be expected.

The interaction between L200E/20 silica and alumina particles is shown in Figure 3. All potentials are attractive throughout the whole range of particle sizes, meaning that, as desired for heterocoagulation, alumina and silica particles will strongly attract each other, leading to an effective coverage of the larger alumina particles by the smaller silica ones. As this coagulation process is barrierless it is expected to be faster than the agglomeration of silica particles, leading to the desired final structure. Concerning the effect of the particles sizes, it can be seen in each of the images in Figure 3 that an increase in the size of alumina particles leads to a more negative potential at most doubling the potential magnitude. Comparing the effect of the silica particle size across the graphs in Figure 3, it is seen to be much more marked, leading to changes of an order of magnitude of the potential values. This implies that the heterocoagulation kinetics are dominated by the size of the smaller silica particles rather than the larger alumina particles in accordance with previous hetero-coagulation models.[35]

4.2. Dispersion Route

The dispersion route is possible in basic conditions, where particles carry surface charges of the same sign, thus repelling each other, which allows the formation of stable suspensions. To evaluate the stability, the interaction potentials between L200A/40 silica (stable under basic conditions) and alumina particles without presence of the PAA surfactant was calculated at pH 10 (zeta potentials Al_2O_3: −17 mV, SiO_2: −31 mV), the results being shown in Figure 4. All pairs attract each other at very small surface separations <1–3 nm; however, an energy barrier will hinder particles approaching each other. For the largest alumina particles, a shallow secondary minimum starts to appear at separations beyond 13 nm. The primary maxima are well below the rather large barriers (>20 kT) calculated for long term stability of these nanoparticle suspensions and agglomeration is to be expected. To maintain the particles well dispersed, the addition of an additive

Downloaded By: [EPFL Lausanne] At: 10:13 25 March 2011

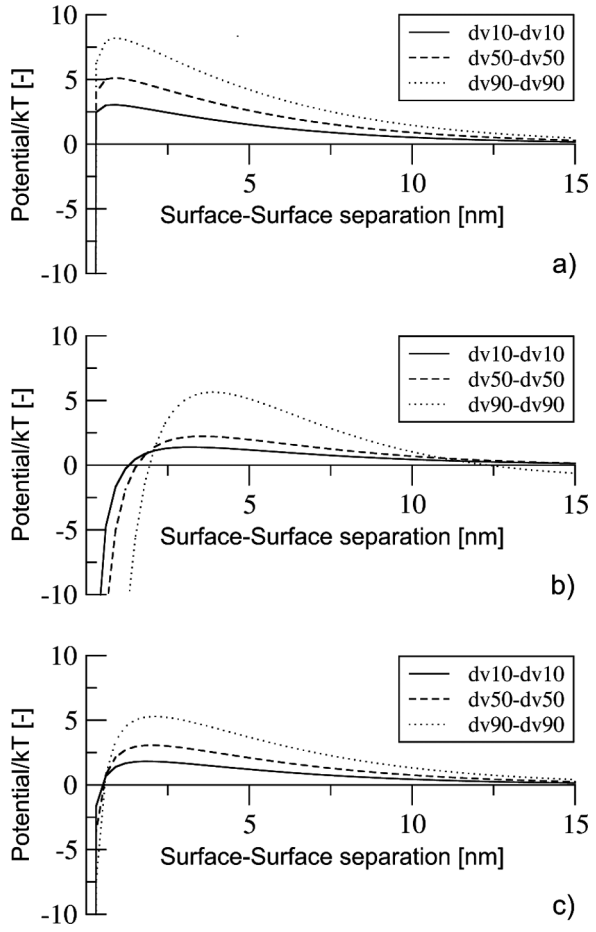

FIG. 4. Interparticle interaction potential for different diameter pairs of a) silica-silica, b) alumina-alumina, and c) silica-alumina.

forming an adsorbed layer thicker than 3 nm or an increase in the magnitude of the zeta potential can be used to close the primary minima. Here, we study the effect of a polyacrylic acid (PAA) polyelectrolyte solution, which should provide both a steric barrier and enhance the electrostatic repulsion due to the charge carried by the additive PAA under basic conditions. To account for this modification in surface charge, the zeta potentials were measured for the particles in presence of PAA (Figure 5). The addition of the negatively charged dispersant notably increases the zeta potential of alumina particles, shifting the IEP into the acidic domain and presenting zeta potential values well below -30 mV at pH > 5, but does not affect the L200A/40 silica as it has a high negatively charged surface potential preventing the adsorption of the negative PAA molecules.

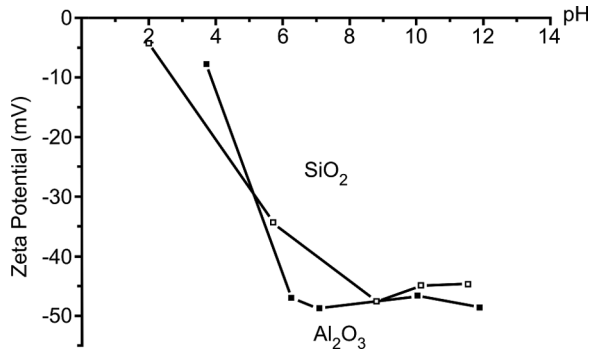

FIG. 5. Zeta potential of L200E/20 silica and alumina in presence of 4% wt PAA.

The volume fraction of PAA in the adsorbed layer depends on the amount of PAA added as well as the working pH. Bowen et al.[9] performed a detailed study of PAA adsorption in the alumina powders used in this work. The pH will affect both the surface charge as well as the degree of dissociation of the PAA molecules. At a pH higher than the IEP of the clean alumina surface (IEP = 8.4, Figure 1) the alumina surface charge is negative and the molecule is completely deprotonated, which also leads to a negative charge. Since the surface and the additive carry the same charge, there are only a few favorable adsorption sites and the additive is expected to adsorb in a brush or mushroom configuration,[30] the maximum amount of polymer at the surface being limited to 1 wt%. At intermediate pH conditions (around 6) alumina surfaces are charged positive, while the additive is still partially dissociated (charged negative), thus enhancing adsorption. The increased number of adsorption sites will lead toward the pancake configuration.[30] Higher amounts of added PAA are likely the increase the thickness of the adsorbed layer as molecules will adsorb in mixed configurations. Based on these considerations, pH of 8 and a 4 wt% solution of PAA were chosen to achieve stable dispersions by enhancing electrostatic repulsion as well as formation of a $\sim$5 nm thick polymer (volume fraction of polymer 0.85) layer around alumina particles.[9] The stability of the L200E/20 silica can be attributed both to the higher surface charge than the L200A/40 silica (Figure 1) and the presence of a 1 nm thick "hydrous" layer on the surface of the particles.[36,37]

In presence of either an adsorbed polymer or the "hydrous" layer, the plane of origin of the electrostatic interaction is situated anywhere in between the particle surface and the outer extremity of the layer. We fix it here to the center of the surface layer (2.5 nm for alumina and 0.5 nm for silica).

Taking into account these parameters, the total interaction potentials were recalculated including the effects of the electrosteric stabilization, the results being shown in Figure 6. As it can be seen the electrosteric approach is very effective, completely eliminating the primary minima for all particle pairs. The magnitude of the potential at large separations is dominated by electrostatics and increases with increasing particle size. Below the interpenetration distance, steric repulsion force dominates, leading to

Downloaded By: [EPFL Lausanne] At: 10:13 25 March 2011

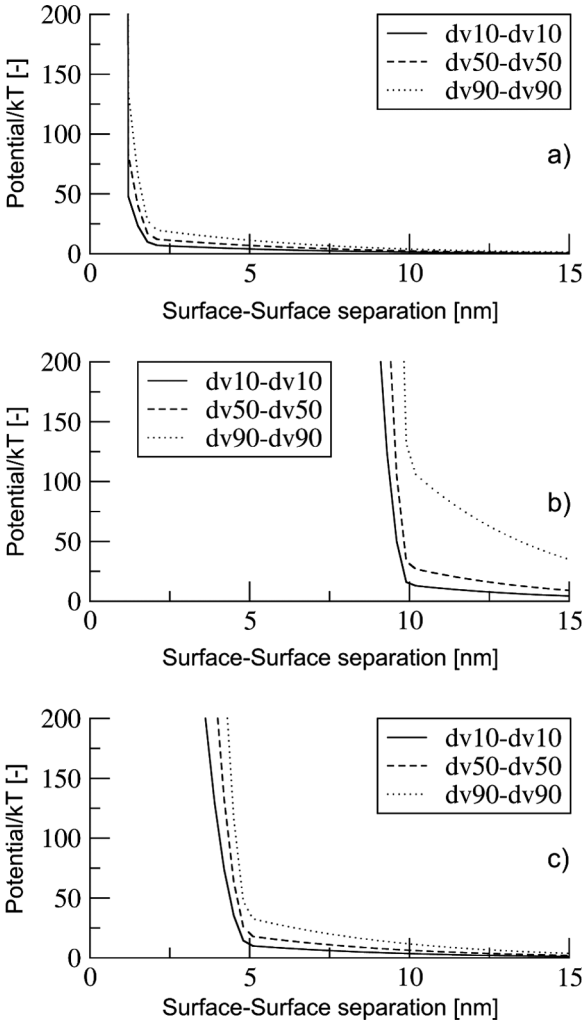

FIG. 6. Interaction potentials for a) silica-silica, b) alumina-alumina, and c) silica-alumina pairs in presence of a 5 nm PAA electrosteric layer on the alumina particles.

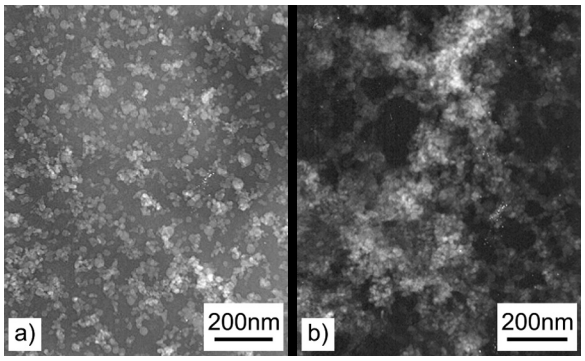

FIG. 7. SEM images of a) the coagulated powder and b) the dispersed powder.

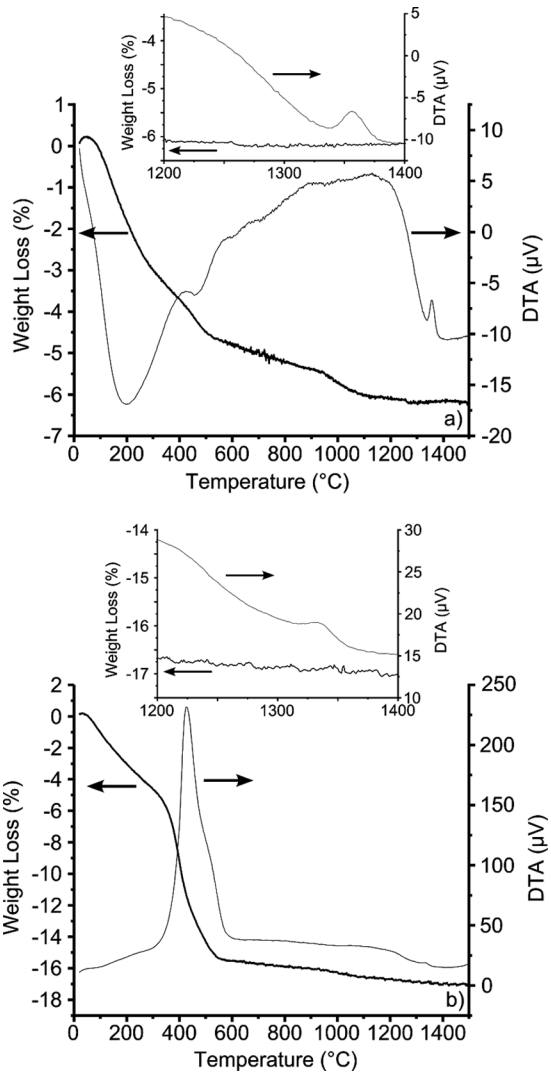

FIG. 8. TG-DTA analysis of the powder obtained by a) heterocoagulation and b) dispersion synthesis. The insets show in more detail the region of mullite formation.

infinitely repulsive potentials. The electrosteric stabilization by PAA is very effective at obtaining well dispersed suspensions of nanosized silica and alumina particles, allowing an intimate mixing in the dispersed state, which should result in powders of good homogeneity after drying.

4.3. Experimental Results

Colloidal silica suspensions were added to the milled alumina suspensions under both heterocoagulation and dispersion conditions and the resulting suspensions were freeze dried for 30 hours. The dry powders obtained from coagulated and dispersed suspensions have high specific surface areas of $104\,m^2/g$ and $99\,m^2/g$ respectively and are shown in Figure 7.

For the coagulated powder, one can mainly see well isolated particles of about 40 nm, which indicates that the smaller silica coated the larger alumina particles forming

Downloaded By: [EPFL Lausanne] At: 10:13 25 March 2011

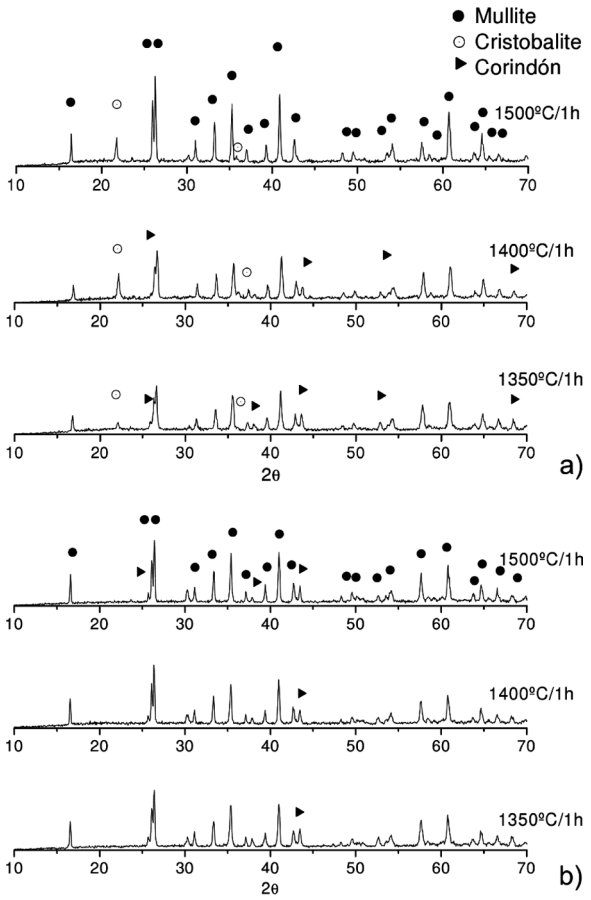

FIG. 9. XRD of a) coagulated powders and b) dispersed powders after thermal treatment at 1350°C, 1400°C, and 1500°C.

the desired core-shell morphology. In the dispersed case an interconnected structure of agglomerates is observed.

For the coagulated powder, thermogravimetric analysis (DTA-TG; Figure 8a) shows loss of intra- and intermolecular water as well as nitrates below 600°C, leading to a net weight loss of about 5%. At 1350°C a peak is observed, which corresponds to mullite formation. For the dispersed powder (Figure 8b) the marked weight loss of about 11% between 300°C and 600°C is attributed to the elimination of PAA. At 1350°C a small mullite transformation peak appears, which is however not as well defined as for the coagulated powder.

Based on these results the powders were treated at the mullite formation temperature (1350°C) and above (1400°C, 1500°C) to further favor the reaction of silica and alumina particles. X-ray diffraction patters for the coagulated and dispersed powders are shown in Figures 9a and b, respectively after thermal treatments at the above mentioned temperatures.

At 1350°C both synthesized powders show a doublet at 27° typical for the mullite phase, although alumina and silica residuals are still clearly present. With increasing temperature the mullite signature increases and at 1500°C silica and alumina have completely reacted. Both methods therefore allow mullite formation at relatively low temperatures (1350°C) but require higher temperatures (1500°C) for complete transformation. The main difference between the two methods can be seen in the stoichiometry of the mullite formed after reaction at 1500°C. For the heterocoagulated powder a slight excess of silica can be detected, whereas for the dispersion route an important deficiency in silica is observed (20 wt% according to ICP-AES measurements). In the dispersed suspension the nanometric silica particles are isolated and can escape during sublimation in the freeze-drying stage, leading to important inhomogeneities in the mullite powder and impeding precise control of the stoichiometry during synthesis. For the heterocoagulation route however the fine silica particles are attached to the much coarser alumina particles by strong electrostatic forces, effectively preventing escape of silica particles. The specific surface areas of the mullite powders are 1.8 m^2/g (d_{BET} 936 nm) and 0.1 m^2/g (d_{BET} 17 μm) for the heterocoagulation and dispersion route respectively. Given that the temperatures required for mullite formation are similar, the heterocoagulation route is thus more suitable for the synthesis of mullite as it allows an intimate mixing by the formation of a core-shell structure. The primary particles of mullite powder with d_{BET} 936 nm from the heterocoagulation route are promising for ceramic processing.

5. CONCLUSIONS

The functions implemented in the Hamaker software were outlined and their application and prospect in understanding and optimizing a ceramic production route demonstrated for the example of mullite formation by reaction of silica and alumina powders. This theoretical approach allows rapid gaining of important understanding of the often delicate force balance in suspensions of ceramic powders.

REFERENCES

[1] Sigmund, W.M., Bell, N.S., and Bergstrom, L. (2000) *J. Amer. Ceramic Soc.*, 83: 1557–1574.
[2] Krell, A., Blank, P., Ma, H.W., Hutzler, T., and Nebelung, M. (2003) *J. Amer. Ceramic Soc.*, 86: 546–553.
[3] Krell, A. and Klimke, J. (2006) *J. Amer. Ceramic Soc.*, 89: 1985–1992.
[4] Nass, R., Aslan, M., Nonninger, R., Schmidt, H., and Matje, P. (1995) In *Ceramic Transactions, Volume 51*, edited by H. Hausner, G.L. Messing, and S.-I. Hirano; Westerville, OH: American Ceramic Society; pp. 433–437.
[5] Bowen, P., Hofmann, H., Staiger, M., Steiger, R., Brugger, P.A., and Peternell, K. (2002) Key Engineering Materials,

Downloaded By: [EPFL Lausanne] At: 10:13 25 March 2011

Euro Ceramics VII, Trans Tech Publications, Zürich, Switzerland (Volumes 206–213): 1977–1980.
[6] Thiele, E.S., Damjanovic, D., and Setter, N. (2001) *J. Amer. Ceramic Soc.*, 84: 2863–2868.
[7] Houst, Y.F., Bowen, P., Perche, F., Kauppi, A., Borget, P., Galmiche, L., Le Meins, J.F., Lafuma, F., Flatt, R.J., Schober, I., Banfill, P.F.G., Swift, D.S., Myrvold, B.O., Petersen, B.G., and Reknes, K. (2008) *Cement Concr. Res.*, 38: 1197–1209.
[8] Palacios, M., Puertas, F., Bowen, P., and Houst, Y.F. (2009) *J. Mater. Sci.*, 44: 2714–2723.
[9] Bowen, P., Carry, C., Luxembourg, D., and Hofmann, H. (2005) *Powder Technol.*, 157: 100–107.
[10] Flatt, R.J. and Bowen, P. (2006) *J. Amer. Ceramic Soc.*, 89: 1244–1256.
[11] Flatt, R.J. and Bowen, P. (2007) *J. Amer. Ceramic Soc.*, 90: 1038–1044.
[12] Strauss, M., Ring, T., Bleier, A., and Bowen, H.K. (1985) *J. Appl. Phys.*, 58: 3871–3879.
[13] Gutierrez, C.A. and Moreno, R. (2003) *British Ceramic Transactions*, 102: 219–224.
[14] Burgos-Montes, O., Nieto, M.I., and Moreno, R. (2007) *Ceramics International*, 33: 327–332.
[15] Russel, W.B., Saville, D.A., and Schowalter, W.R. (1985) *Colloidal Dispersions*; Cambridge, UK: Cambridge Press.
[16] Derjaguin, B. and Landau, L. (1941) *Acta Physico Chemica URSS*, 14: 633–662.
[17] Verwey, E.J.W. and Overbeek, J.T.G. (1948) *Theory of the Stability of Lyophobic Colloids*; Amsterdam: Elsevier.
[18] Hamaker, H.C. (1937) *Physica*, 4: 1058–1072.
[19] Bergstrom, L. (1997) *Adv. Colloid Interface Sci.*, 70: 125–169.
[20] French, R.H., Cannon, R.M., DeNoyer, L.K., and Chiang, Y.-M. (1995) *Solid State Ionics*, 75: 13–33.
[21] Vincent, B. (1973) *J. Colloid Interface Sci.*, 42: 270–285.
[22] Gregory, J. (1981) *J. Colloid Interface Sci.*, 83: 138–145.
[23] Bowen, W.R. and Jenner, F. (1995) *Adv. Colloid Interface Sci.*, 56: 201–243.
[24] Evans, D.F. and Wennerström, H. (1999) *The Colloidal Domain*; New York: Wiley-VCH.
[25] Hogg, R., Healy, T.W., and Fuerstenau, D.W. (1966) *Trans. Faraday Soc.*, 62: 1638–1651.
[26] Bell, G.M., Levine, S., and McCartney, L.N. (1970) *J. Colloid Interface Sci.*, 33: 335–359.
[27] Napper, D.H. (1983) *Polymeric Stabilization of Colloidal Dispersions*; London: Academic Press.
[28] Buscall, R., McGowan, I.J., and Mumme-Young, C.A. (1990) *Faraday Discussions*, 90: 115–127.
[29] Bergstrom, L., Schilling, C.H., and Aksay, I.A. (1992) *J. Amer. Ceramic Soc.*, 75: 3305–3314.
[30] de Gennes, P.G. (1987) *Adv. Colloid Interface Sci.*, 27: 189–209.
[31] Israelachvili, J.N. (1991) *Intermolecular and Surface Forces*; San Diego: Academic Press.
[32] Somiya, S., Davies, R.F., and Pask, J.A., (eds.) (1990) *Mullite and Mullite Matrix Composites, Ceramic Transactions, Vol. 6*; Westerville, OH: American Ceramic Society.
[33] Aksay, I.A., Dabbs, D.M., and Sarikaya, M. (1991) *J. Amer. Ceramic Soc.*, 74: 2343–2358.
[34] Bowen, P. (2002) *J. Dispersion Sci. Technol.*, 23: 631–662.
[35] Kim, S. and Zukoski, C.F. (1990) *J. Colloid Interface Sci.*, 139: 198–212.
[36] Kobayashi, M., Juillerat, F., Galletto, P., Bowen, P., and Borkovec, M. (2005) *Langmuir*, 21: 5761–5769.
[37] Juillerat, F., Bowen, P., and Hofmann, H. (2006) *Langmuir*, 22: 2249–2257.

Downloaded By: [EPFL Lausanne] At: 10:13 25 March 2011